



Solvent-free selective oxidation of alcohols by molecular oxygen over gold nanoparticles supported on β -MnO₂ nanorods

Lu-Cun Wang, Lin He, Qian Liu, Yong-Mei Liu, Miao Chen, Yong Cao^{*}, He-Yong He, Kang-Nian Fan

Department of Chemistry & Shanghai Key Laboratory of Molecular Catalysis and Innovative Materials, Fudan University, Shanghai 200433, PR China

ARTICLE INFO

Article history:

Received 13 December 2007

Received in revised form 9 April 2008

Accepted 11 April 2008

Available online 20 April 2008

Keywords:

Gold
 β -MnO₂ nanorods
 Solvent-free
 Aerobic
 Alcohol oxidation

ABSTRACT

The performances of a series of MnO₂-supported gold nanocatalysts with varying gold loading were studied in the solvent-free selective oxidation of alcohols by molecular oxygen. The gold was deposited onto the β -MnO₂ support, featuring one dimensional rod-like morphology, by means of homogeneous deposition–precipitation. The catalytic activity of the catalyst for the solvent-free aerobic oxidation of benzyl alcohol was found to increase with increasing gold loading, with the highest specific activity in terms of turnover frequencies (TOF) being achieved over the catalyst with 5 wt.% gold loading. Both XRD and TEM results showed that the majority of Au particles of various catalysts have diameters in the range of 2–6 nm. Temperature-programmed reduction (TPR) results indicated that the reducibility of MnO₂ was significantly enhanced with the surface-deposited gold nanoparticles. X-ray photoelectron spectroscopy (XPS) revealed the coexistence of both oxidized and metallic gold species on the surface of MnO₂, the composition of which depends critically on the gold loading. The superior specific activity of the catalyst with 5% gold loading was attributed to the presence of higher amounts of positive gold species and more surface oxygen vacancy sites resulting from stronger metal–support interactions as compared to other catalysts.

© 2008 Elsevier B.V. All rights reserved.

1. Introduction

The selective oxidation of alcohols is one of the most fundamental transformations in organic chemistry for both laboratory and industrial manufacturing [1,2]. Traditionally, numerous oxidizing reagents including dichromate and permanganate have been employed in order to accomplish this transformation. However, these stoichiometric oxidants have serious drawbacks; for instance, they are expensive and many have serious toxicity issues associated with them [1]. With ever-increasing environmental concerns, intense research efforts have been devoted to develop efficient catalytic procedures that use molecular oxygen (O₂) as a primary oxidant, for it is readily available and produces water as the sole byproduct [2]. In this context, a great number of noble metal-catalyzed aerobic processes have been developed over the last decades [3–6].

Gold nanoparticles or nanoclusters supported on activated carbon, oxides or polymers have attracted considerable recent attention in the oxidation of alcohols owing to their higher selectivity and lower proneness to leaching compared to their conventional noble metal counterparts [7–18]. Of the reported

systems, the combination of gold nanoparticles and metal oxides has been extensively explored for the liquid-phase aerobic oxidation of alcohols into their corresponding aldehydes or ketones under solvent-free and base-free conditions [9–15]. Moreover, it has been shown that the choice of a suitable metal oxide as support plays an important role in determining the catalytic activity and selectivity of the gold catalyst. For example, Abad et al. have recently reported that Au nanoparticles supported on nanocrystalline CeO₂ gave a highly active, selective and recyclable catalyst for solvent-free oxidation of alcohols under mild conditions [9,10]. Enache et al. have shown that very high activity for aerobic alcohol oxidation could be achieved by using Au or Au–Pd catalysts supported on TiO₂ [11,12]. More recently, gold catalysts deposited on U₃O₈ [13], and Cu–Mg–Al mixed oxides [14] were also claimed to be active and selective for aerobic alcohol oxidation.

Manganese oxide has superior ability to activate and supply oxygen, so it is well known as a stoichiometric oxidant for oxidation of hydrocarbons or alcohols in organic synthesis and has also been extensively investigated as an excellent support or promoter for various metal or metal oxide catalysts [19–24]. When combined with gold nanoparticles, significantly enhanced activity has been achieved over Au/MnO_x system for low-temperature CO oxidation in the absence or presence of H₂ for fuel cell applications. However, to the best of our knowledge, manganese oxide has

^{*} Corresponding author. Tel.: +86 21 55665287; fax: +86 21 65642978.
 E-mail address: yongcao@fudan.edu.cn (Y. Cao).

rarely been investigated as support of gold particles in the catalytic alcohol oxidation [13,24]. In the present work, we report the selective oxidation of various structurally different alcohols under solvent-free conditions over nanosized gold catalysts by using MnO₂ nanorods as the support material. The effects of gold loading on the structural and catalytic properties of the MnO₂-supported Au catalysts are investigated. The structure–activity relationships of the Au/MnO₂-R materials are discussed in light of a detailed characterization of the physicochemical and surface properties of the catalysts.

2. Experimental

2.1. Preparation of supports and catalysts

The β-MnO₂ nanorods were prepared by a hydrothermal method according to [25]. Briefly, MnSO₄·H₂O (0.016 mol) and an equal amount of ammonium persulfate ((NH₄)₂S₂O₈) were put into distilled water at room temperature to form a homogeneous solution, which was then transferred into a 100-mL Teflon-lined stainless-steel autoclave. This autoclave was sealed and maintained at 140 °C for 24 h. After the reaction was completed, the resulting solid product was recovered by filtration and by washing four times with distilled water, followed by drying at 100 °C overnight.

Gold was deposited on the as-synthesized β-MnO₂ nanorods (denoted as xAu/MnO₂-R, x stands for the gold loading in weight percent) by homogeneous deposition–precipitation (HDP) using urea as the precipitating agent. In a typical procedure, 3.6 g urea was dissolved in 200 mL of 1.46 mmol L⁻¹ HAuCl₄ solution at room temperature. MnO₂ support is then added to this solution. The temperature of the resulting slurry is increased gradually to 90 °C and maintained for 4 h. The solid mass is filtered, washed several times with distilled water, dried and then calcined at 300 °C for 4 h in static air.

2.2. Catalyst characterization

The BET specific surface areas of the calcined catalysts were determined by adsorption–desorption of nitrogen at liquid nitrogen temperature, using Micromeritics TriStar 3000 equipment. Sample degassing was carried out at 300 °C prior to acquiring the adsorption isotherm.

Elemental analysis with respect to Au loading was performed using ion-coupled plasma atomic emission spectroscopy (ICP-AES) on a Thermo Electron IRIS Intrepid II XSP spectrometer. The samples were dissolved in a mixture of concentrated HCl and HNO₃ with a volumetric ratio of 3/1 prior to the analysis.

Transmission electron microscopy (TEM) images were recorded on a JEOL 2011 electron microscope operating at 200 kV. Before being transferred into the TEM chamber, the samples dispersed with ethanol were deposited onto a carbon-coated copper grid and then quickly moved into the vacuum evaporator.

The X-ray powder diffraction (XRD) of the samples was carried out on a Bruker D8 advance X-ray diffractometer using nickel filtered Cu Kα radiation with a voltage of 40 kV and a current of 20 mA.

Temperature-programmed reduction (TPR) profiles were obtained on a homemade apparatus loaded with 20 mg of catalyst. TPR experiments were carried out in 5% H₂/Ar flowing at 40 mL min⁻¹, with a ramping rate of 10 °C min⁻¹ to a final temperature of 650 °C. The H₂ consumption was monitored using a TCD detector.

X-ray photoelectron spectroscopy (XPS) spectra were recorded with a PerkinElmer PHI 5000C system equipped with a hemispherical electron energy analyzer. The Mg Kα ($h\nu = 1253.6$ eV) was operated at 15 kV and 20 mA. The binding energy (BE)

scale was referenced to the C 1s peak (284.6 eV) arising from adventitious carbon in the sample.

2.3. Catalytic activity tests

The liquid-phase aerobic oxidation of alcohols was carried out in a high-pressure, Teflon-lined, stainless-steel autoclave reactor (Dalian Tongchan Co. Ltd., China; 200 mL). Then, 0.2 g of the catalyst was transferred to the catalytic reactor that had been charged with 200 mmol of alcohol. The reactor was sealed and purged five times with oxygen leaving the vessel at the desired pressure. The consumed O₂ was replenished by maintaining the oxygen pressure constant throughout the experiment. The magnetic stirring speed was set at 1200 rpm and the reaction mixture was raised to the required temperature. Samples were taken periodically during the reaction. The products were separated by centrifuging, and analyzed with a gas chromatograph (Trace GC Ultra) fitted with a HP-5 capillary column (25 m × 0.32 mm) and flame ionization detector (FID). The conversions and selectivities were determined using undecane as an internal standard in all reactions. The average turnover frequencies (TOF) for the catalysts with different gold loadings were calculated based on conversion at $t = 5$ h; the number of surface gold atoms was evaluated by assuming a hemi-sphere model of the exposed gold nanoparticles.

3. Results and discussion

3.1. Structural and textural properties of the catalysts

The gold contents of various Au/MnO₂-R catalysts were determined by ICP-AES. Results given in Table 1 shows that the measured gold content was essentially the same as the nominal loading for all catalysts, confirming the effectiveness of the urea-mediated Au deposition onto the MnO₂ support [26]. The as-synthesized β-MnO₂ nanorods has a BET surface area (S_{BET}) of 25 m² g⁻¹. When gold was deposited onto the surface of MnO₂ nanorods, a slightly reduced BET surface area was identified. On increasing the Au loading from 1 to 8%, the surface area of the Au/MnO₂-R catalyst decreased monotonously from 24 to 17 m² g⁻¹.

The XRD patterns of pure MnO₂ nanorods and of the 5Au/MnO₂-R catalyst are shown in Fig. 1. The MnO₂ material have diffraction features characteristic of the β-MnO₂ phase (JCPDS 24-0735). After the deposition of gold nanoparticles on the surface of MnO₂ nanorod support, the XRD patterns remain unchanged, although weak metallic gold peaks are evidenced, in particular for the more highly loaded samples. However, it should be noted that the diffraction peaks due to metallic gold are too weak to determine the average crystallite size (smaller than 5 nm) by Sherrer's equation. This result also indicates that the homogeneous deposition–precipitation method employed in this study can allow the fabrication of Au/MnO₂ catalysts with very small gold

Table 1

Gold loadings, BET surface areas, mean gold particle sizes and the reduction peak maxima of various catalysts

Sample	Au loading (wt.%) ^a	BET surface area (m ² g ⁻¹)	d_{Au} (nm) ^b	T_{M} (°C) ^c
MnO ₂ -R	–	25	–	325
1Au/MnO ₂ -R	1.0	24	3.2	276
3Au/MnO ₂ -R	3.0	21	3.9	205
5Au/MnO ₂ -R	5.0	18	4.3	179
8Au/MnO ₂ -R	7.9	17	5.1	189

^a Determined by ICP-AES analysis.

^b Average gold particle size estimated by statistical analysis from TEM results.

^c Reduction peak maxima in the TPR profiles.

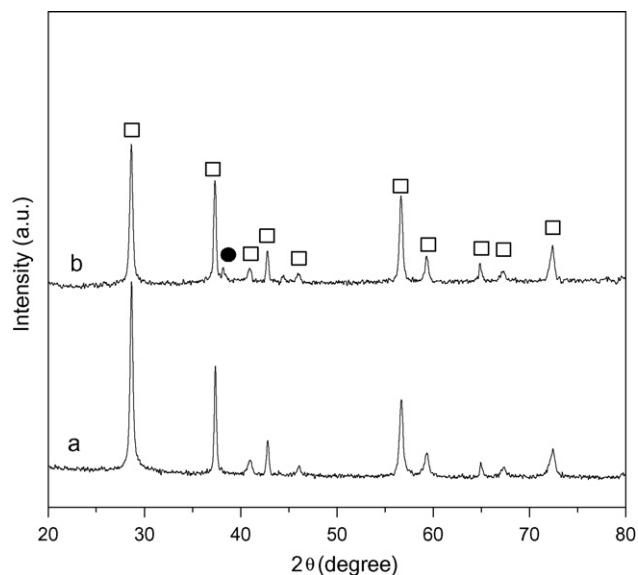


Fig. 1. XRD patterns of (a) $\text{MnO}_2\text{-R}$ and (b) $5\text{Au}/\text{MnO}_2\text{-R}$. (\square) $\beta\text{-MnO}_2$ and (\bullet) metallic gold.

nanoparticles highly dispersed on the surface of MnO_2 support in a wide range of gold loadings (up to 8%).

To overcome the limitations of the XRD technique, we obtained the TEM images of gold catalysts supported on MnO_2 nanorods with different gold loadings; these images are shown in Fig. 2. It can be seen that the $\text{MnO}_2\text{-R}$ support has well-defined rod-like morphology with diameters of 40–100 nm and lengths ranging between 2.5 and 4.0 μm [25]. TEM images of the Au-containing MnO_2 nanorod materials (Fig. 2) reveal a narrow size distribution of the gold particles deposited on the surface of the MnO_2 nanorods, especially for the low-loading samples. The sizes of most gold nanoparticles are in the range of 2–6 nm. Accordingly, the mean gold particle sizes are estimated to be 3.2, 3.9, 4.3 and 5.1 nm for the $\text{Au}/\text{MnO}_2\text{-R}$ catalysts with gold loadings of 1, 3, 5 and 8%,

respectively. The increased gold particle size at higher gold loadings may be caused by the relatively low surface area of the $\text{MnO}_2\text{-R}$ support and the reduced distance between gold nanoparticles, which induced the agglomeration of gold particles.

3.2. Redox properties and chemical states

TPR experiments were carried out to investigate the reducibility of various MnO_2 -supported catalysts. Fig. 3 presents the reduction profiles of various $\text{Au}/\text{MnO}_2\text{-R}$ catalysts. For comparison, the TPR profile of pure $\text{MnO}_2\text{-R}$ is also included. Two reduction peaks can be identified for all five samples, indicating the stepwise reduction of manganese oxides [27]. According to the literature, the low-temperature (LT) peak should be attributed to the reduction of MnO_2 to Mn_3O_4 , whereas the high-temperature (HT) peak should be attributed to the consecutive reduction of Mn_3O_4 to MnO [27]. With the introduction of 1% Au, the LT reduction peak catalyst shifted appreciably from 325 to 276 $^\circ\text{C}$. The reduction of MnO_2 has also been shown to be strongly facilitated by the presence of Ag [28] and Rh [29]; such improved reduction was attributed to the occurrence of spillover phenomena involving hydrogen activated on the metal phase. In our case, the TPR results clearly demonstrate that the presence of Au nanoparticles strongly promotes MnO_2 reduction due to the beneficial metal–support interactions.

With increasing gold loading, a progressive shift of the reduction peak maxima (T_M) to lower temperature is observed (see Table 1). Notably, the lowest reduction temperature was achieved for the sample containing 5% Au. When we further increased the gold content to 8%, the main reduction peak shifted towards higher temperatures. This indicates that an optimized metal–support interaction between gold and MnO_2 support was achieved in the $5\text{Au}/\text{MnO}_2\text{-R}$ catalyst. The higher temperature of the reduction peak for $8\text{Au}/\text{MnO}_2\text{-R}$ catalyst may be caused by the increase of the gold particle size, which results in diminished metal–support interaction between Au and MnO_2 nanorods.

The surface composition and oxidation state of the catalyst were investigated by XPS. Fig. 4 shows the representative Au 4f core level XPS spectrum of the $5\text{Au}/\text{MnO}_2\text{-R}$ catalyst. The detailed

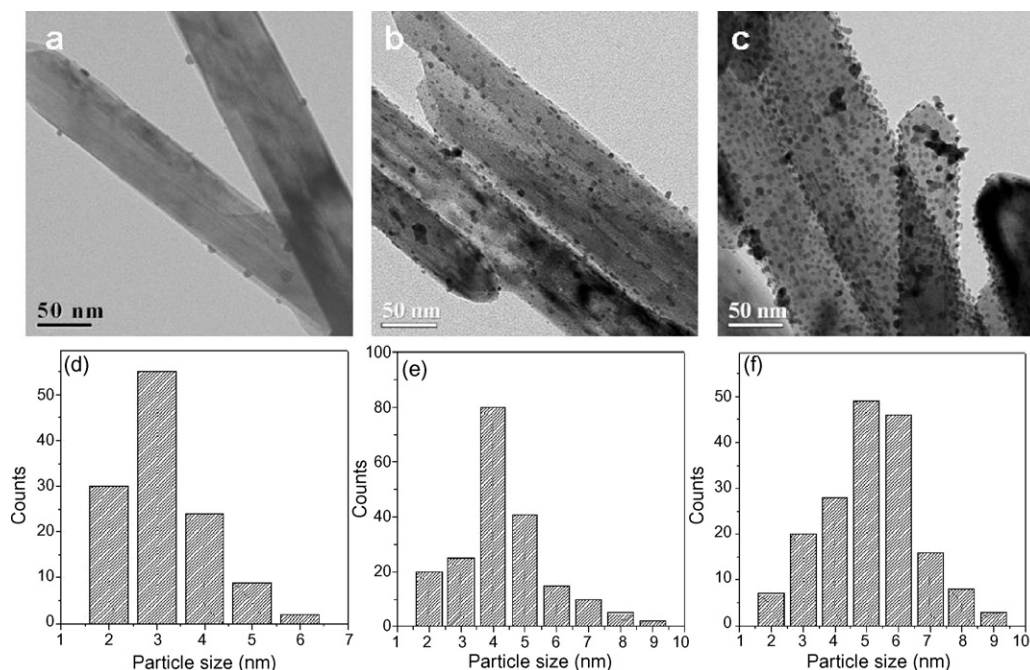


Fig. 2. Representative TEM images and gold particle size distributions of (a and d) $1\text{Au}/\text{MnO}_2\text{-R}$, (b and e) $5\text{Au}/\text{MnO}_2\text{-R}$ and (c and f) $8\text{Au}/\text{MnO}_2\text{-R}$.

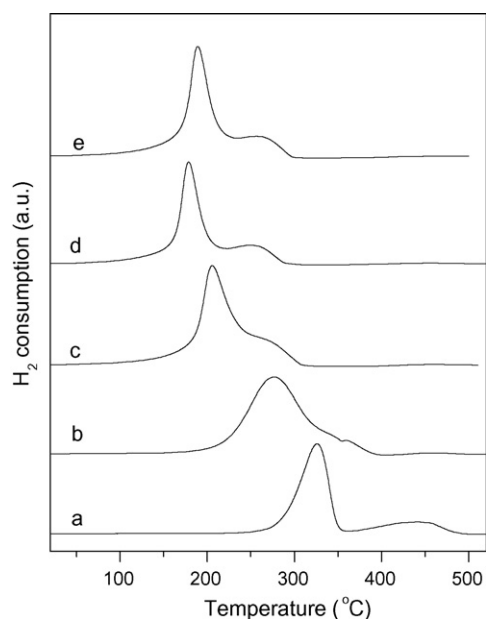


Fig. 3. TPR profiles of (a) MnO₂-R, (b) 1Au/MnO₂-R, (c) 3Au/MnO₂-R, (d) 5Au/MnO₂-R and (e) 8Au/MnO₂-R.

XPS parameters of all samples are summarized in Table 2. Broad peaks of Au 4f_{7/2} and Au 4f_{5/2} states were observed in all Au/MnO₂ samples, indicating the presence of both metallic and ionic gold species [30,31]. Table 2 presents the deconvolution analysis results of the Au 4f spectra of various catalysts. It can be seen that in addition to the main peak characteristic of metallic Au⁰, the XPS spectra also contain the 4f_{7/2} signals from Au^{δ+} ions [32–34]. When the gold loading was increased from 1 to 5%, the relative portion of Au^{δ+} species in the Au/MnO₂-R catalyst increased progressively from ca. 12.4 to 18.5%. Furthermore, it is worthwhile to mention that oxidized gold species (ca. 15.6%) were also detected on the surface of 5Au/MnO₂-R catalyst after reaction for 8 h in the solvent-free oxidation of benzyl alcohol. Similar to our findings, Abad et al. have recently shown by XPS and IR spectroscopy the presence of positive gold ions in Au/CeO₂ catalyst [9]. Such species has been suggested to be of vital importance in the rate-controlling step during the oxidation of alcohols involving the hydride shift from the alcohol to gold [10,35].

Fig. 5 shows the Mn 2p XPS spectra of various MnO₂-supported gold catalysts. The data indicate that the Mn 2p_{3/2} peaks of both MnO₂-R and Au/MnO₂-R samples have a binding energy of about 642.1 eV, which is in good agreement with those reported in the literature for MnO₂, i.e., 642 ± 0.2 eV [36]. Moreover, a weak shoulder can be identified at ca. 646 eV, the intensity of which is slightly increased for catalysts with higher gold loadings, as indicated

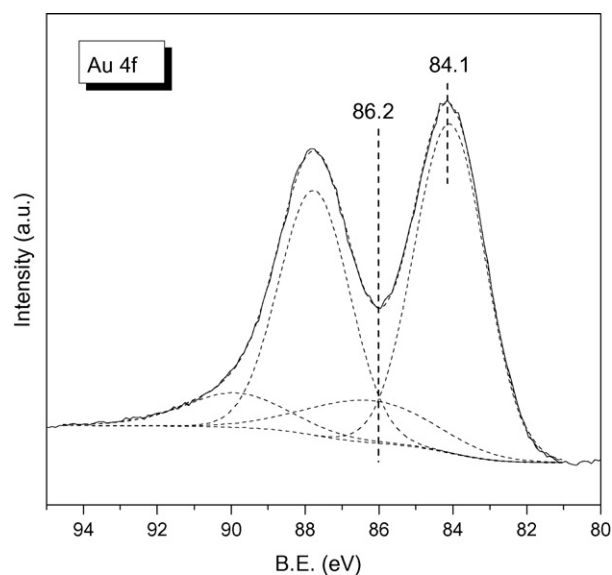


Fig. 4. Representative Au 4f XPS spectra of 5Au/MnO₂-R.

by the arrow. This shoulder feature is due to the presence of Mn species associated with lower valence states, i.e., MnO or Mn₃O₄ [37]. This result points to the presence of oxygen vacancies on the surfaces of Au/MnO₂-R catalysts.

Fig. 6 shows the O 1s XPS spectra obtained from pure MnO₂ and from various MnO₂-supported gold catalysts. The O 1s main peak at ca. 528.7 eV is attributed to the lattice oxygen molecules bonded to Mn atoms [38]. In addition, distinct shoulders are visible on the high binding energy sides of the main peaks. Similar shoulder features have also been observed in the O 1s XPS spectra of Au/MnO_x catalysts prepared by aqueous coprecipitation; such features were assigned to a mixture of hydroxyl groups and adsorbed water on the surface of catalysts [39]. As shown in Fig. 6, with the introduction of gold, the intensities of the shoulder features at higher binding energies significantly increased, pointing to the enrichment of hydroxyl groups and an accumulation of adsorbed water on the surface induced by the gold–support interaction. With increasing gold content, the amount of surface adsorbed water and hydroxyl groups increases; the trend is consistent with the variation of positively charged gold species shown above. It is therefore reasonable to infer that these increasing oxygen-containing groups are relevant to the formation of oxidized gold species, which are suggested to be essential for the high activity in the process of alcohol oxidation [9,10,16].

The surface O/Mn atomic ratios of various Au/MnO₂-R catalysts summarized in Table 2 indicates that the surface compositions are strongly affected by the gold loading level. The molar ratio of the

Table 2
XPS results of Au/MnO₂-R catalysts with different gold loadings

Catalyst	Binding energy of Au 4f _{7/2} (eV)	Fraction of Au species (%)	Binding energy of Mn 2p _{3/2} (eV)	O _T /Mn molar ratio ^a	O _L /Mn molar ratio ^b
MnO ₂ -R	–	–	–	2.3	1.7
1Au/MnO ₂ -R	84.0	87.6	642.0	3.0	1.6
3Au/MnO ₂ -R	84.1	85.0	642.1	3.6	1.6
5Au/MnO ₂ -R	84.1	81.5	642.2	4.2	1.4
8Au/MnO ₂ -R	84.1	87.1	642.2	5.3	1.5
	85.8	12.9			

^a O_T: total surface oxygen.

^b O_L: surface lattice oxygen.

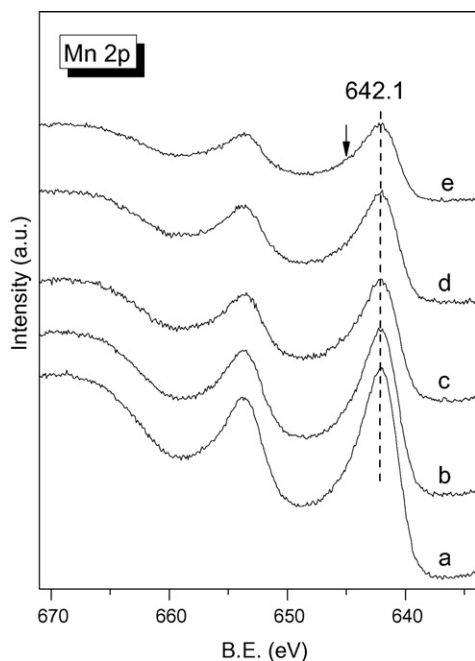


Fig. 5. Mn 2p XPS spectra of (a) $\text{MnO}_2\text{-R}$, (b) $1\text{Au/MnO}_2\text{-R}$, (c) $3\text{Au/MnO}_2\text{-R}$, (d) $5\text{Au/MnO}_2\text{-R}$ and (e) $8\text{Au/MnO}_2\text{-R}$.

total amount of surface oxygen (O_T) to Mn is significantly higher than the stoichiometric value of MnO_2 ; this fact further confirms the presence of a high concentration of hydroxyl groups or adsorbed water on the surfaces of the $\text{Au/MnO}_2\text{-R}$ catalysts. On the other hand, the molar ratios of surface lattice oxygen (O_L , 528.7 eV) to Mn for all samples are smaller than the stoichiometric value, in line with the conclusion obtained from Mn 2p XPS spectra, indicating the existence of surface oxygen vacancies. Meanwhile, the data show that catalyst $5\text{Au/MnO}_2\text{-R}$ has the highest concentration of surface oxygen vacancies. This observation, together with the TPR results, further confirmed the presence of an optimized metal–support interaction in $5\text{Au/MnO}_2\text{-R}$ as compared

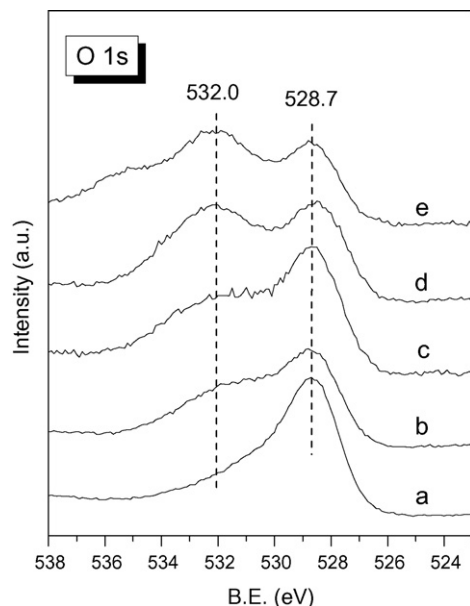


Fig. 6. O 1s XPS spectra of (a) $\text{MnO}_2\text{-R}$, (b) $1\text{Au/MnO}_2\text{-R}$, (c) $3\text{Au/MnO}_2\text{-R}$, (d) $5\text{Au/MnO}_2\text{-R}$ and (e) $8\text{Au/MnO}_2\text{-R}$.

to other samples. It has been suggested that, for Au/CeO_2 catalyst, the presence of nanosized gold particles can cause a strong modification of the support [40,41]. This modification results in facile oxygen vacancies' formation and an enhanced electron transfer between the support and the small gold particles, which accounts for the high activity of the catalyst. We believe that a similar modification effect is also present in the $\text{Au/MnO}_2\text{-R}$ system to a larger extent for the $5\text{Au/MnO}_2\text{-R}$ catalyst. This may explain the enhanced alcohol oxidation activity observed for this catalyst, as shown in the following section.

3.3. Solvent-free aerobic oxidation of alcohols

For the MnO_2 -supported gold catalysts, our initial studies focused on the solvent-free aerobic oxidation of benzyl alcohol, because this reaction is often employed as a model reaction for alcohol oxidation [11–13]. Furthermore, this substrate has relatively high reactivity and the main product is a non-enolizable aldehyde, thus reducing the number of possible side products [14]. In all cases, benzaldehyde was obtained as the major product, and only small amounts of other product, viz., benzyl benzoate, was observed. On the other hand, control experiments using the parent $\text{MnO}_2\text{-R}$ support (substrate to $\text{MnO}_2 \sim 100$) in the absence of gold reveal that only less than 2% of the benzyl alcohol can be selectively converted to benzaldehyde within 5 h at 120°C . All these results allow us to confirm the stoichiometric oxidant nature of the present MnO_2 materials as well as the essential role of Au for catalytic alcohol oxidation.

Fig. 7 shows a typical set of results for benzyl alcohol conversion over the $5\text{Au/MnO}_2\text{-R}$ catalyst, illustrating the dependence of conversion and selectivity on the reaction time. As the reaction proceeded, the conversion of benzyl alcohol and the selectivity to benzyl benzoate increased, while the selectivity to benzaldehyde decreased. Abad et al. have shown by ^1H NMR spectroscopy that the ester was directly formed via the hemiacetal intermediate [9]. However, one cannot deny the possibility that the instant reaction between benzoic acid (the over oxidized product) and the reactant (benzyl alcohol) may also contribute to some extent toward the ester formation, as suggested by Choudhary et al.

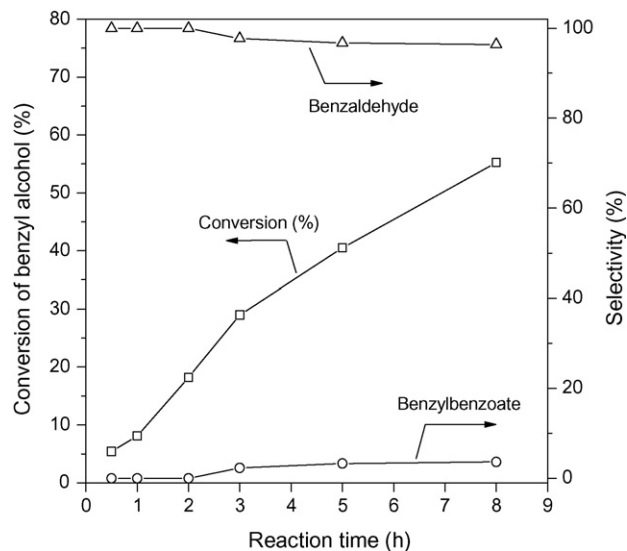


Fig. 7. The catalytic performance of $5\text{Au/MnO}_2\text{-R}$ catalyst as a function of reaction time. Reaction conditions: 0.2 g catalyst, 200 mmol benzyl alcohol, 0.3 MPa O_2 and 120°C .

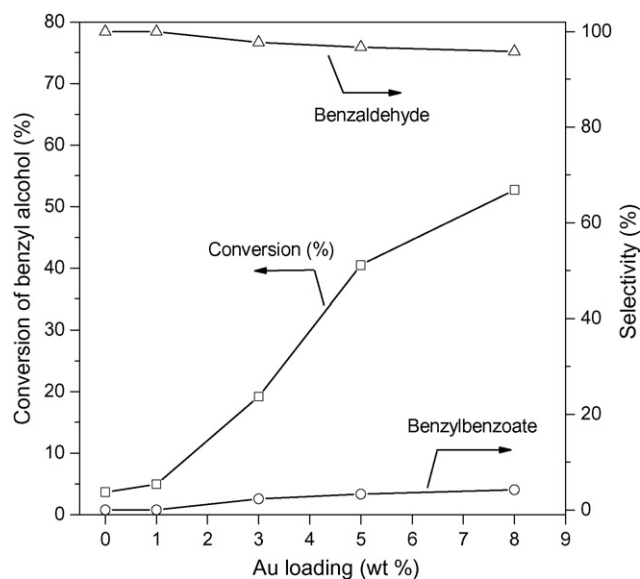


Fig. 8. The effect of gold loading on the catalytic performance of Au/MnO₂-R catalyst. Reaction conditions: 0.2 g catalyst, 200 mmol benzyl alcohol, 0.3 MPa O₂, 120 °C, after reaction for 5 h.

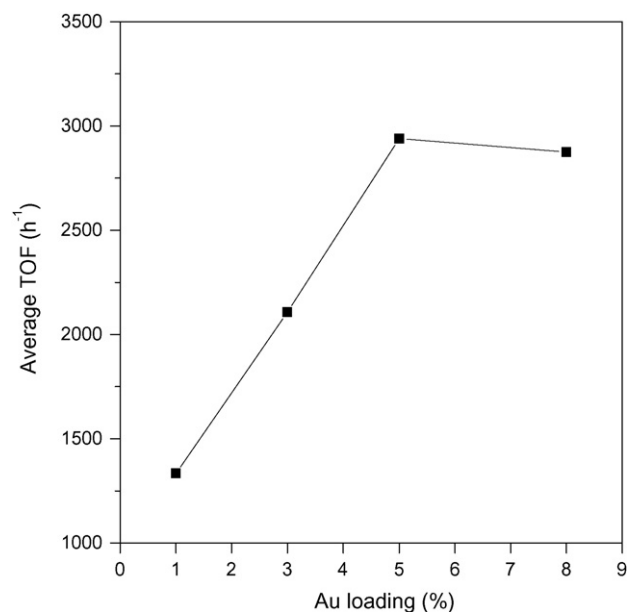


Fig. 9. The average TOF as a function of gold loading. Reaction conditions: 0.2 g catalyst, 200 mmol benzyl alcohol, 0.3 MPa O₂, 120 °C, after reaction for 5 h.

[13]. Moreover, it can be seen that the conversion rate of benzyl alcohol was very high at the initial stage of the reaction; this rate continuously decreased as the reaction period became longer. This result may be caused by several factors, e.g. the decreased concentration of benzyl alcohol, the adsorption of reaction products on the surface of the catalyst [2] or even the deactivation of the catalyst. A similar trend was also reported in the solvent-free oxidation of benzyl alcohol with Au/TiO₂ and Au-Pd/TiO₂ catalysts by Hutchings and co-workers [11,12].

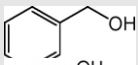
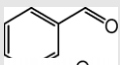
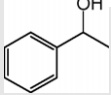
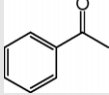
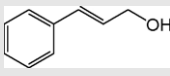
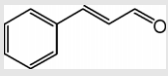
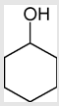
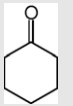


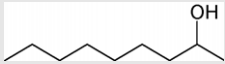

It is also interesting to make a further comparison of the four catalysts with different gold loadings. Presumably, the conversion of benzyl alcohol should increase linearly with the gold loading if gold acts as the sole active site for the oxidation reaction. However, Fig. 8 shows that with increasing gold loading, the conversion of benzyl alcohol increases drastically, almost exponentially, and when the gold loading exceeds 5%, the conversion increased to a less extent. To gain a further insight into the effect of gold loading on the intrinsic activity of the Au/MnO₂-R catalyst, we calculated the average TOF for each catalyst; the results are depicted in Fig. 9. The TOF was found to increase with gold loading up to 5% and to decrease with further increase of the gold loading. This result unambiguously demonstrates that the MnO₂ support also plays an important role in the catalytic oxidation process via more beneficial metal-support interactions. Very recently, Abad et al. have demonstrated that the catalytic activity of Au/CeO₂ catalyst for aerobic alcohol oxidation is dramatically reduced if the free ceria surface is covered by an excess amount of gold species [35]. The essential role of the free ceria surface is suggested to act as an oxygen pump, ensuring the facile oxidation of metal hydrides into water [35]. In this respect, it appears that the free surfaces of the MnO₂ nanorods may also play a role for the aerobic alcohol oxidation reaction.

The scope of the most active 5Au/MnO₂-R catalyst for a range of structurally different alcohols has also been investigated. The catalytic results are summarized in Table 3. It is apparent that the Au/MnO₂-R catalyst showed a higher reactivity for benzylic and allylic alcohols than for aliphatic ones. Under similar reaction conditions, the oxidation of 1-phenylethanol gave the highest yield (80.9%, entry 2) for 8 h. In the oxidation of cinnamyl alcohol, a

model reaction for α,β -unsaturated alcohols, C=C double bonds remained intact without an intramolecular hydrogen transfer (Table 3, entry 3). Unfortunately, cyclohexanol and 1-octanol appeared to be poor substrates, yielding the corresponding carbonyl compounds in only 10.7% (Table 3, entry 4) and 2.4% (Table 3, entry 5) yields for 8 h, respectively. In addition, the primary linear aliphatic alcohol 1-octanol showed a lower activity compared with the secondary aliphatic alcohol 2-octanol (Table 3, entry 6) and the primary alcohol gives predominantly the corresponding ester with high selectivity, accompanied by lesser amounts of the aldehyde. These results are consistent with those obtained over Au/CeO₂ and Au-Pd/C catalysts reported by Abad et al. [9] and Dimitratos et al. [42], respectively. Moreover, it is worth noting that the 5Au/MnO₂-R catalyst is very active in the oxidation of 2-octanol, for which the Au-Pd/TiO₂ catalyst is totally inactive even at high temperatures despite its high activities in the oxidation of other secondary alcohols, such as 3-octanol [12]. This difference may be due to the specific interactions of this substrate with the active site [12].

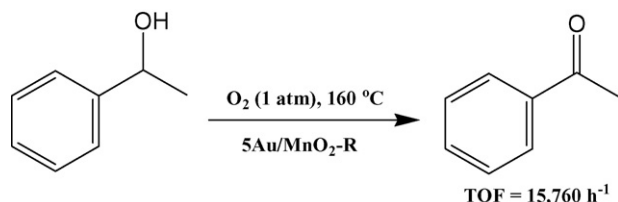
Enache et al. [12] and Abad et al. [10] have recently reported very high TOF values in the solvent-free oxidation of 1-phenylethanol at 160 °C with Au-Pd/TiO₂ (TOF = 26,900 h⁻¹) and Au/CeO₂ (TOF = 12,500 h⁻¹) catalysts, respectively. Under similar reaction conditions, a TOF value comparable with that of Au/CeO₂ catalyst was also recently achieved over a ternary-mixed-oxide supported gold catalyst Au/Cu₅Mg₁Al₂O_x (TOF = 11,748 h⁻¹) by Haider and Baiker [14]. In this study, to compare with other reported catalysts, they also investigated the catalytic performance of the 5Au/MnO₂-R catalyst in the solvent-free aerobic oxidation of 1-phenylethanol at 160 °C under atmospheric pressure (see Scheme 1). Although the specific experimental conditions in the references concerning the selective oxidation of alcohols may deviate from each other, a rough comparison is still feasible. The results showed that the 5Au/MnO₂-R catalyst exhibited a specific rate of 15,760 h⁻¹ under similar reaction conditions. This value compares favorably with the results reported on Au/CeO₂ or Au/Cu₅Mg₁Al₂O_x catalysts [10,14], demonstrating that the present catalytic system can serve as a promising catalyst for the selective oxidation of alcohols.

Table 3
Solvent-free oxidation of various alcohols with oxygen over 5Au/MnO₂-R catalyst^a

Entry	Substrate	Product	t (h)	Conversion (%)	Selectivity (%)	Yield (%)	TOF (h ⁻¹) ^b
1			8	55.3	96.9	53.6	320
2			8	80.9	100	80.9	1324
3			10	72.1	97.0	69.9	284
4			8	10.8	99.5	10.7	225
5			8	20.0	12.0	2.4	401
6			10	55.7	100	55.7	295

^a Reaction conditions: 120 °C, 0.3 MPa, 0.2 g catalyst and 200 mmol substrate.

^b Initial TOFs are calculated based on the conversion at t = 1 h and the total amount of Au present in the sample.



Scheme 1. Solventless, atmospheric-pressure oxidation of (±)-1-phenylethanol by molecular oxygen in the presence of the 5Au/MnO₂-R catalyst. Reaction conditions: (±)-1-phenylethanol (200 mmol), 1.3 × 10⁻³ mol.% (substrate to catalyst ratio). The TOF for the initial 0.5 h of reaction is calculated by dividing the initial reaction rate to the number of catalytic sites. Initial reaction rates can be obtained from the slope of the time–conversion plot at zero time. [10].

4. Conclusion

In this study, gold nanoparticles were deposited on MnO₂ nanorod materials with different gold loadings by a HDP method. The catalysts were tested in the liquid-phase aerobic oxidation of benzyl alcohol under solvent-free conditions. The catalytic activity tests show that the activity of Au/MnO₂-R catalyst depends strongly on the gold loading and that the 5Au/MnO₂-R catalyst exhibited the highest specific activity in terms of TOF. This catalyst was also tested in the oxidation of various structurally different alcohols. For most of the alcohols, high selectivities (≥97%) to the corresponding aldehydes or ketones were achieved. TPR results indicated that the presence of Au strongly promotes MnO₂ reduction in the Au/MnO₂-R system. XPS revealed the coexistence of both oxidized and metallic gold species on the surface of MnO₂, the composition of which depends substantially on the gold loading. It is proposed that the optimized metal–support interaction and the presence of the higher amount of positive gold species account for the highest specific activity achieved for the 5Au/MnO₂-R catalyst.

Acknowledgments

This work was supported by the NSF of China (20421303, 20473021 and 20633030), the State Key Basic Research Program of PRC (2003CB615807), the National High Technology Research and

Development Program of China (2006AA03Z336), the Shanghai Science & Technology Committee (07QH14003) and Shanghai Education Committee (06SG03).

References

- [1] R.A. Sheldon, I.W.C.E. Arends, A. Dijkman, *Catal. Today* 57 (2000) 157–166.
- [2] T. Mallat, A. Baiker, *Chem. Rev.* 104 (2004) 3037–3058.
- [3] K. Mori, K. Yamaguchi, T. Hara, T. Mizugaki, K. Ebitani, K. Kaneda, *J. Am. Chem. Soc.* 124 (2002) 11572–11573.
- [4] T. Nishimura, T. Onoue, K. Ohe, S. Uemura, *J. Org. Chem.* 64 (1999) 6750–6755.
- [5] M. Hasan, M. Musawir, P.N. Davey, I.V. Kozhevnikov, *J. Mol. Catal. A: Chem.* 180 (2002) 77–84.
- [6] K. Yamaguchi, K. Mori, T. Mizugaki, K. Ebitani, K. Kaneda, *J. Am. Chem. Soc.* 122 (2000) 7144–7145.
- [7] A.S.K. Hashmi, G.J. Hutchings, *Angew. Chem. Int. Ed.* 45 (2007) 7896–7936.
- [8] F. Porta, L. Prati, *J. Catal.* 224 (2004) 397–403.
- [9] A. Abad, P. Concepcion, A. Corma, H. Garcia, *Angew. Chem. Int. Ed.* 44 (2005) 4066–4069.
- [10] A. Abad, C. Almela, A. Corma, H. Garcia, *Tetrahedron* 62 (2006) 6666–6672.
- [11] D.I. Enache, D.W. Knight, G.J. Hutchings, *Catal. Lett.* 103 (2005) 43–52.
- [12] D.I. Enache, J.K. Edwards, P. Landon, B. Solsona-Espriu, A.F. Carley, A.A. Herzing, M. Watanabe, C.J. Kiely, D.W. Knight, G.J. Hutchings, *Science* 311 (2006) 362–365.
- [13] V.R. Choudhary, A. Dhar, P. Jana, R. Jha, B.S. Uphade, *Green Chem.* 7 (2005) 768–770.
- [14] P. Haider, A. Baiker, *J. Catal.* 248 (2007) 175–187.
- [15] C. Milone, R. Ingoglia, G. Neri, A. Pistone, S. Galvagno, *Appl. Catal. A: Gen.* 211 (2001) 251–257.
- [16] A.N. Pstryakov, V.V. Lunin, *J. Mol. Catal. A: Chem.* 158 (2000) 325–329.
- [17] J. Hu, L. Chen, K. Zhu, A. Suchopar, R. Richards, *Catal. Today* 122 (2007) 277–283.
- [18] H. Miyamura, R. Matsubara, Y. Miyazaki, S. Kobayashi, *Angew. Chem. Int. Ed.* 46 (2007) 4151–4154.
- [19] L. Singoredjo, R. Korver, F. Kapteijn, J. Moulijn, *Appl. Catal. B: Environ.* 1 (1992) 297–316.
- [20] F. Morales, E. de Smit, F.M.F. de Groot, T. Visser, B.M. Weckhuysen, *J. Catal.* 246 (2007) 91–99.
- [21] G.G. Xia, Y.G. Yin, W.S. Willis, J.Y. Wang, S.L. Suib, *J. Catal.* 185 (1999) 91–105.
- [22] R. Radhakrishnan, S.T. Oyama, *J. Phys. Chem. B* 105 (2001) 4245–4253.
- [23] Y.F. Han, F. Chen, Z. Zhong, K. Ramesh, L. Chen, E. Widjaja, *J. Phys. Chem. B* 110 (2006) 24450–24456.
- [24] R.M.T. Sanchez, A. Ueda, K. Tanaka, M. Haruta, *J. Catal.* 168 (1997) 125–127.
- [25] X. Wang, Y.D. Li, *Chem. Eur. J.* 9 (2003) 300–306.
- [26] R. Zanella, S. Giorgio, C.R. Henry, C. Louis, *J. Phys. Chem. B* 106 (2002) 7634–7642.
- [27] E.R. Stobbe, B.A. de Boer, J.W. Geus, *Catal. Today* 47 (1999) 161–167.
- [28] R. Xu, X. Wang, D. Wang, K. Zhou, Y. Li, *J. Catal.* 237 (2006) 426–430.
- [29] H. Trevino, G.D. Lei, W.M.H. Sachtler, *J. Catal.* 154 (1995) 245–252.
- [30] M. Haruta, N. Yamada, T. Kobayashi, S. Iijima, *J. Catal.* 115 (1989) 301–309.
- [31] W.S. Epling, G.B. Hoflund, J.F. Weaver, *J. Phys. Chem.* 100 (1996) 9929–9934.
- [32] S. Minicò, S. Scire, C. Crisafulli, S. Galvagno, *Appl. Catal. B: Environ.* 34 (2001) 277–285.

- [33] J.M.C. Soares, P. Morrall, A. Crossley, P. Harris, M. Bowker, *J. Catal.* 219 (2003) 17–24.
- [34] L. Fan, N. Ichikuni, S. Shimazu, T. Uematsu, *Appl. Catal. A: Gen.* 246 (2003) 87–95.
- [35] A. Abad, A. Corma, H. Garcia, *Chem. Eur. J.* 28 (2007) 212–222.
- [36] F. Kapteijn, A.D. van Langeveld, J.A. Moulijn, A. Andreini, M.A. Vuurman, A.M. Turek, J.M. Jehng, I.E. Wachs, *J. Catal.* 150 (1994) 94–104.
- [37] B. Srinivasan, S.D. Gardner, *Surf. Interface Anal.* 26 (1998) 1035–1049.
- [38] S.D. Gardner, G.B. Hoflund, M.R. Davidson, *Langmuir* 7 (1991) 2140–2145.
- [39] S.J. Lee, A. Gavriilidis, Q.A. Pankhurst, A. Kyek, F.E. Wagner, P.C.L. Wong, K.L. Yeung, *J. Catal.* 200 (2001) 298–308.
- [40] D. Andreeva, R. Nedyalkova, L. Ilievaa, M.V. Abrashev, *Appl. Catal. B: Environ.* 52 (2004) 157–165.
- [41] D. Andreeva, P. Petrova, J.W. Sobczak, L. Ilieva, M. Abrashev, *Appl. Catal. B: Environ.* 67 (2006) 237–245.
- [42] N. Dimitratos, A. Villa, D. Wang, F. Porta, D. Su, L. Prati, *J. Catal.* 244 (2006) 113–121.